nature
structural biology

Coupling of light-induced electron transfer to proton uptake in photosynthesis

André Remy & Klaus Gerwert

Light energy is transformed into chemical energy in photosynthesis by coupling a light-induced electron transfer to proton uptake. The resulting proton gradient drives ATP synthesis. In this study, we monitored the light-induced reactions in a 100-kDa photosynthetic protein from 30 ns to 35 s by FTIR difference spectroscopy. The results provide detailed mechanistic insights into the electron and proton transfer reactions of the Q_A to Q_B transition: reduction of Q_A in picoseconds induces protonation of histidines, probably of His126 and His128 in the H subunit at the entrance of the proton uptake channel, and of Asp210 in the L subunit inside the channel at 12 μs and 150 μs. This seems to be a prerequisite for the reduction of Q_B, mainly at 150 μs. Q_A^- is reoxidized at 1.1 ms, and a proton is transferred from Asp210 to Glu212 in the L subunit, the proton donor to Q_B^-. Notably, our data indicate that Q_B is not reduced directly by Q_A^- but presumably through an intermediary electron donor.

Sun energy is transformed into chemical energy by photosynthesis, which sustains most forms of life on earth. Generally, sunlight oxidizes a primary donor such as a chlorophyll molecule within a photosynthetic protein complex. The released electron is then transferred within the same complex to a final electron acceptor, typically a quinone molecule. The subsequent protonation of the reduced quinone is the first step in a series of events to create a proton gradient that drives ATP synthesis[1]. Here we used time-resolved Fourier transform infrared (FTIR) difference spectroscopy[2–5] to study when and how light-induced electron transfer is coupled to proton uptake in a photosynthetic protein complex at the atomic level.

The system used in this study is the photosynthetic reaction center (RC) from the purple nonsulfur bacterium *Rhodobacter* (*Rb.*) *sphaeroides*[6], a system structurally very similar to the photosystem II in higher plants[7]. This bacterial RC is a transmembrane pigment protein complex of ~100 kDa, the three-dimensional structure of which has been determined at up to 2.2-Å resolution[6,8–10]. Upon light excitation, an electron is transferred from the primary donor P (bacteriochlorophyll *a* dimer) via the intermediate acceptors bacteriochlorophyll (A) and bacteriopheophytin (I) to the primary quinone Q_A and finally to the secondary quinone Q_B (**Fig. 1**).

In *Rb. sphaeroides* ubiquinone-10 (UQ_{10}) is bound both at Q_A and at Q_B. At Q_A, UQ_{10} accepts one electron and transfers it to Q_B. At Q_B, UQ_{10} accepts two electrons and two protons and is finally released from the RC in the fully reduced form (Q_BH_2) (for a recent review see ref. 1). Different hydrogen bonding of the 4-C=O quinone groups to the protein governs the different roles of UQ_{10} at Q_A and Q_B[11–14].

The electron transfer from the primary donor P to the primary acceptor Q_A takes place in ~200 ps (ref. 15). From P down to Q_A, the chromophore orbitals overlap and thereby provide a fast electron transfer chain (**Fig. 1**). In contrast, the following $Q_A^-Q_B \rightarrow Q_AQ_B^-$ transition is 10^6 times slower. There is no obvious conduction chain between Q_A and Q_B as observed between P and Q_A, and it is not clear which groups are involved in the electron transfer across the ~20 Å center-to-center distance from Q_A to Q_B. There is currently a debate as to whether electron transfer takes place through bonds or through space[16,17]. An involvement of the nonheme Fe^{2+} positioned between Q_A and Q_B has been excluded based on visible and ultraviolet photolysis (UV-VIS) studies of Fe-depleted RCs[18]. The $Q_A^-Q_B \rightarrow Q_AQ_B^-$ transition has been described as containing two kinetic phases with

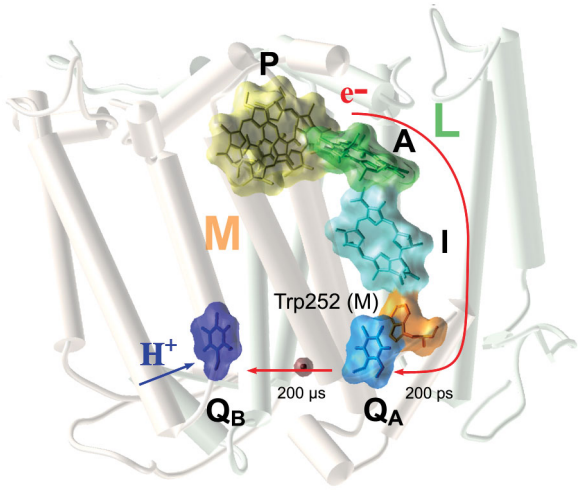

Figure 1 Light-induced electron transfer from P to Q_A takes place within 200 ps via overlapping prosthetic groups. The $Q_A^-Q_B \rightarrow Q_AQ_B^-$ transition is ~10^6-fold slower. The doubly reduced Q_B is protonated from the external medium.

Lehrstuhl für Biophysik, Ruhr-Universität Bochum, Postfach 102148, 44780 Bochum, Germany. Correspondence should be addressed to K.G. (gerwert@bph.ruhr-uni-bochum.de).

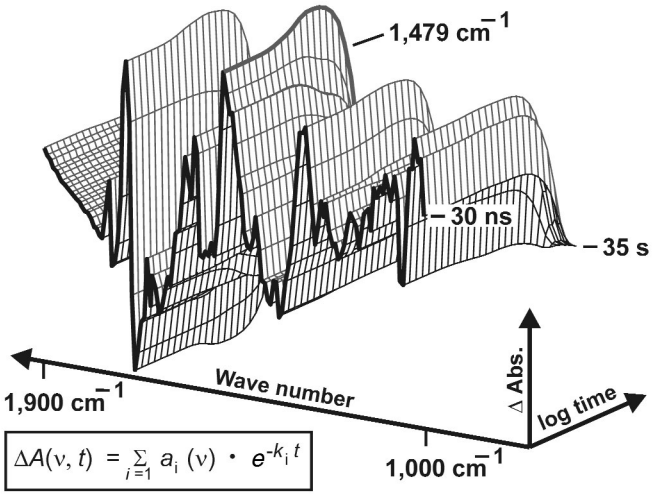

Figure 2 Three-dimensional representation of the light-induced IR absorbance changes in the photosynthetic reaction center of *Rb. sphaeroides* between 1,900 and 1,000 cm^{-1} with 30-ns time resolution and 7-cm^{-1} spectral resolution as revealed by global fit analysis. The time axis has a logarithmic scale to show the complete reaction over nine orders of magnitude (from 30 ns to 35 s) in one representation.

time constants in the ranges of 25–67 μs and 200–250 μs at 295 K on the basis of UV-VIS studies[19–22]. These studies have assigned the fast phase to electron transfer and the slow phase to charge compensation, proton uptake and conformational relaxation of the protein[19–22]. However, UV-VIS and near infrared (NIR) measurements detect global chromophore changes and do not provide information about the individual residues involved in the process. By contrast, IR spectroscopy can distinguish between the chromophore moieties, amino acid side chains and protein backbone groups that participate in a reaction[23]. A first IR investigation using tunable IR diode lasers with 0.5-μs time resolution has yielded two kinetic phases of 120–180 μs and 1.0–1.2 ms at 277 K (refs. 24,25), in agreement with UV-VIS studies at this temperature[21]. However, diode lasers are limited to a narrow spectral range, whereas the FTIR technique, which allows simultaneous data acquisition in the entire middle infrared range from 1,900 to 1,000 cm^{-1}, monitors the absorbance changes of all groups involved in a reaction[26–28]. The first time-resolved step-scan FTIR measurements with 5-μs time resolution have also yielded two kinetic phases (150 μs and 1.2 ms)[29], consistent with previous studies.

Here, we describe improvement in time resolution of the time-resolved step-scan FTIR technique to 30 ns and the use of the technique to monitor the $Q_A^-Q_B \rightarrow Q_AQ_B^-$ transition in the RC with a rotating wheel to measure eight different samples in parallel. This modification allows increased signal averaging to improve the signal-to-noise ratio. The new IR data set provides three time constants and new mechanistic insights into this transition, thereby elucidating the coupling of the electron and the proton transfers in the $Q_A^-Q_B \rightarrow Q_AQ_B^-$ transition.

RESULTS

We monitored the light-induced absorbance changes of the RC between 1,900 and 1,000 cm^{-1} from 30 ns to 35 s (**Fig. 2**). A multi-exponential global fit analysis[30] of the absorbance changes in this spectral range gave six apparent time constants (see Methods): 12 μs, 150 μs, 1.1 ms, 63 ms, 770 ms and 3.1 s at 278 K. Because ~128 spectral elements were analyzed simultaneously in the global fit, the analysis was substantially improved as compared with fits using single-frequency data. In particular, small absorbance changes were more reliably defined. Furthermore, kinetic analyses of narrower spectral regions, such as the amide I region between 1,675 and 1,550 cm^{-1} (protein backbone conformational changes) or the carbonyl region between 1,800 and 1,675 cm^{-1} (protonation changes of carboxylic groups), yielded the same apparent time constants. This showed that all reactions of the different groups within the RC were highly synchronized and excluded uncoupled reactions. This result is in contrast to an earlier proposal for the RC[24], but is in agreement with the observations in bacteriorhodopsin[31] and in the photoactive yellow protein[32].

Recombination from $P^+Q_A^-$ and $P^+Q_B^-$ to P

To illustrate the kinetic analysis and show the data quality, the absorbance change at 1,282 cm^{-1} is presented (**Fig. 3a**). At 1,282 cm^{-1} A P^+ vibration absorbs[33]. In addition, the individual contributions ($\Sigma a_i e^{-k_i t}$) of the apparent time constants are shown (**Fig. 3a**). The time constant for the light-induced formation of P^+ was ~200 ps[15]; this reaction was therefore not resolved in our experiments. The observed signal rise (**Fig. 3a**, crosses) represented the detector response with a time constant of 30 ns. The small oscillation superimposed on the detector response was observed at all frequencies mostly in the nanosecond time range up to ~1 μs; this is an artifact of the detector. Because the oscillation is independent of any specific frequency, it could be extracted computationally. We analyzed the data starting at 150 ns. At 150 ns, P^+ was completely formed, and the absorbance at 1,282 cm^{-1} did not change until finally charge recombination from $P^+Q_A^-$ to P or from $P^+Q_B^-$ to P occurred with time constants of 63 ms or of 770 ms and 3.1 s, respectively (**Fig. 3a**).

Global fit analysis provided time constants τ_i and amplitudes a_i for the kinetic phases over the entire spectral range. The corresponding amplitude spectra a_i represent the absorbance changes accompanying the transition determined by the respective apparent time constant τ_i as a function of frequency. In such spectra only groups undergoing a reaction in the particular transition show absorbance changes, and the entire background absorbance of the protein and the buffer (including water) is eliminated. The amplitude spectrum associated with the 63-ms phase (data not shown) was very similar to the $P^+Q_A^- - PQ_A$ difference spectrum already published[33]. Therefore, this phase represents the $P^+Q_A^- \rightarrow P$ recombination process, in agreement with ref. 34. The amplitude spectra for the two slower phases, at 770 ms and 3.1 s, (data not shown) were similar to $P^+Q_B^- - PQ_B$ difference spectra[33]; these two phases were therefore assigned to the recombination process from $P^+Q_B^-$ to P. The amplitude of the $P^+Q_A^- \rightarrow P$ recombination (63 ms) was ~10% of the entire amplitude (**Fig. 3a**) indicating that 90% of the Q_B is active in the RC used for these measurements in agreement with control measurements in the UV-VIS spectral range (data not shown).

Kinetic analysis of the $Q_A^-Q_B \rightarrow Q_AQ_B^-$ transition

The $Q_A^-Q_B \rightarrow Q_AQ_B^-$ transition can be monitored by the absorbance changes at 1,446 and 1,479 cm^{-1}. These bands have been clearly assigned to the C ⋯ O/C ⋯ C vibrations of Q_A^- and to the 1,4-C ⋯ O stretching mode of Q_B^-, respectively, using site-specific 1-^{13}C- and 4-^{13}C-labeled UQ_{10} reconstituted either at Q_A or Q_B[11–14]. Appearance of these bands indicated reduction, whereas disappearance of these bands indicated oxidation of the quinones at Q_A or Q_B, respectively. Both P^+ and the 1,4-C ⋯ O stretching mode of Q_B^- absorb at 1,479 cm^{-1} (**Fig. 3b**)[13,14]. The absorbance increase of P^+ due to the $P^+Q_A^-$ charge separation in 200 ps and its subsequent relax-

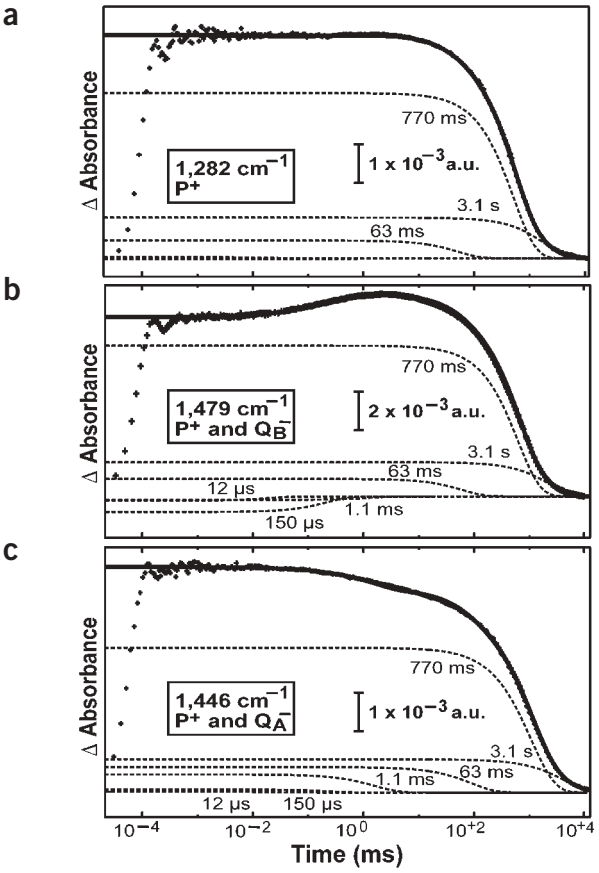

Figure 3 Absorbance changes of P^+, Q_B^- and Q_A^- marker bands. Raw data, crosses; global fit, thick line; contributions of single exponentials, dashed lines. (**a**) Absorbance changes at 1,282 cm^{-1} represent a P^+ vibration. (**b**) Absorbance changes at 1,479 cm^{-1} represent a P^+ vibration and a Q_B^- vibration. An additional increase with three kinetic phases (12 µs, 150 µs and 1.1 ms) is observed. (**c**) Absorbance changes at 1,446 cm^{-1} represent a P^+ vibration as well as a Q_A^- vibration. An additional decrease with three kinetic phases (12 µs, 150 µs and 1.1 ms) is also observed.

ation to the ground state from $P^+Q_A^-$ and from $P^+Q_B^-$ to P with time constants of 63 ms, 770 ms, and 3.1 s were as described above (**Fig. 3a**). In contrast to data at 1,282 cm^{-1}, an additional absorbance increase with three phases at 12 µs, 150 µs and 1.1 ms was observed. Because in addition to P^+, Q_B^- also absorbs at 1,479 cm^{-1}, this additional absorbance increase was caused by reduction of Q_B. The step-scan FTIR experiments therefore indicated that the $Q_A^-Q_B \rightarrow Q_AQ_B^-$ transition should be described by three apparent time constants of 12 µs, 150 µs and 1.1 ms at 278 K.

The absorbance change of the Q_A^- marker band at 1,446 cm^{-1} (**Fig. 3c**) showed that Q_A^- also disappeared with three kinetic phases at 12 µs, 150 µs and 1.1 ms, but with different amplitudes for each time constant. This is better resolved on an enlarged scale in **Figure 4**: the absorbance changes at 1,479 cm^{-1} (for Q_B^-) and at 1,446 cm^{-1} (for Q_A^-) and the contributions to the individual reaction steps are presented in the time window of the $Q_A^-Q_B \rightarrow Q_AQ_B^-$ transition from 1 µs to 10 ms. At 1,479 cm^{-1}, Q_B was reduced mainly with the phase at 150 µs (67%) and partly with the phases at 12 µs (18%) and 1.1 ms (15%), whereas at 1,446 cm^{-1}, Q_A^- was oxidized mainly with the phase at 1.1 ms (82%) and partly with the phase at 150 µs (18%).

The global fit gave apparent time constants. They described—like intrinsic time constants—individual reaction steps only if back reactions could be excluded. As the apparent time constants differ here by one order of magnitude, in a first approximation back reactions can be neglected and the dominating apparent rate describes mostly one reaction step[30]. However, small admixtures of the other reaction steps contribute to each transition described by the apparent rate. Therefore, not only one, but all of the apparent time constants contribute to the absorbance changes at 1,479 cm^{-1} and at 1,446 cm^{-1}, respectively, but with different dominating amplitudes.

Because reduction of Q_B mainly occurred with the 150-µs phase and oxidation of Q_A^- with the 1.1-ms phase, a direct Q_A^- to Q_B electron transfer is unlikely, in contrast to earlier proposals[18]. Thus, an intermediary electron donor X must be involved that first reduces Q_B (at 150 µs) and itself is then reduced by Q_A^- (at 1.1 ms).

At first glance the differences described above did not seem obvious (**Fig. 4a**). This might be why UV-VIS studies have not resolved this issue until now. In addition, in the UV-VIS spectra the bands for Q_A and Q_A^- and for Q_B and Q_B^- were much broader than the IR bands for the same species, and these bands overlap substantially. Therefore, the absorbance changes in the UV-VIS spectral range might not be able to provide as clear kinetics for the $Q_A^-Q_B \rightarrow Q_AQ_B^-$ transition as those in the IR range.

Analysis of the amplitude spectra

To identify the functional groups involved in the $Q_A^-Q_B \rightarrow Q_AQ_B^-$ transition, we examine the amplitude spectra associated with the three kinetic phases at 12 µs, 150 µs and 1.1 ms (**Fig. 5**). The amplitude spectrum for the 12-µs phase (**Fig. 5a**) was about three times smaller than those of the other two phases. Because there were fewer data points in this early time regime, the signal-to-noise ratio of the amplitude spectrum was worse than those for the other two slower phases. The noise level was estimated using the region of 1,900–1,800 cm^{-1} because no absorbance changes of the protein were expected there. Nevertheless, the global fit provided clear evidence for the 12-µs phase: several bands were clearly above the noise level, for example those at 1,751, 1,707 and 1,479 cm^{-1}. Only the amide I region (1,680–1,620 cm^{-1}) might contain artifacts and should be interpreted with caution because of large background absorbance from the amide bonds and from water.

Quinone vibrations

The amplitude spectrum for the 12-µs phase (**Fig. 5a**) contained a rather small band at 1,479 cm^{-1}. It represents a Q_B^- marker band because the position of this band shifted when 4-^{13}C-labeled UQ_{10} was reconstituted at Q_B[13]. The intensity of this band was much higher in the amplitude spectrum for the 150-µs phase (**Fig. 5b**). Therefore, we assigned most of the reduction of Q_B to the 150-µs phase. The absorbance of Q_B^- at 1,479 cm^{-1} changed little in the 1.1-ms phase (**Fig. 5c**). As discussed above, the smaller Q_B^- bands in the 12-µs and 1.1-ms phases seemed to reflect contributions of the back reactions.

There was no Q_A^- band in the amplitude spectrum for the 12-µs phase (**Fig. 5a**). Rather small intensities for Q_A^- bands at 1,466 and 1,447 cm^{-1} appeared in the 150-µs phase (**Fig. 5b**). The positions of these bands shifted when 4-^{13}C-labeled UQ_{10} was reconstituted at Q_A (ref. 11). The band at 1,456 cm^{-1} does not correspond to a semiquinone vibration mode and probably represents a protein group[11,12]. The disappearance of large Q_A^- bands at 1,466 and 1,447 cm^{-1} dominated the amplitude spectrum for the 1.1-ms phase (**Fig. 5c**). Therefore we assigned the major oxidation of Q_A^- to the 1.1-ms phase.

In principle, the intensities of the C=C and C=O bands in Q_A and Q_B can also be used to monitor the concentration of these species. In

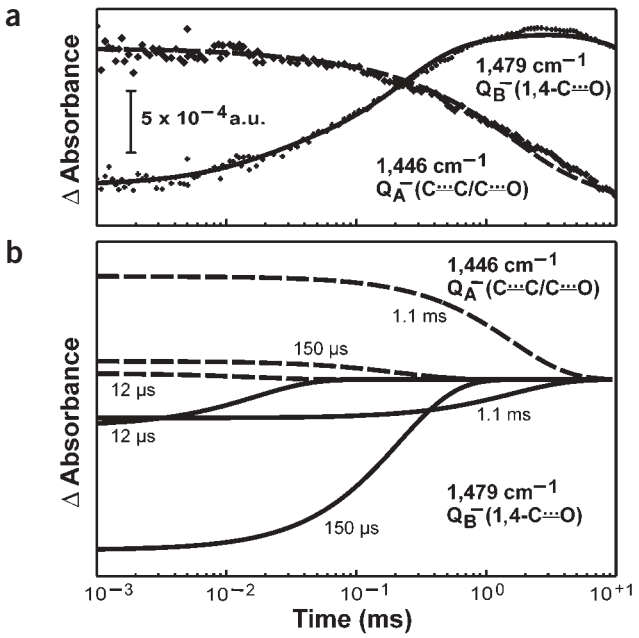

Figure 4 On an expanded scale the $Q_A^-Q_B \rightarrow Q_AQ_B^-$ transition is shown from 1 µs to 10 ms. The absorbance changes, (**a**) the global fit and (**b**) the respective contributions of the exponentials to the absorbance changes at 1,479 cm^{-1} of Q_B^- (solid lines) and at 1,446 cm^{-1} of Q_A^- (hatched lines).

particular, Brudler *et al.*[13] have identified two populations of UQ_{10} at Q_B in the dark: a minor fraction (30%) shows weak protein interactions because its 1,4-C=O vibrations absorb at 1,664 and 1,651 cm^{-1} as observed for UQ_{10} free in solution, and a major population (70%) shows symmetric hydrogen bonds to the protein as indicated by a single carbonyl band at 1,641 cm^{-1}.

In the amplitude spectrum of the 12-µs phase (**Fig. 5a**) the disappearing carbonyl bands of UQ_{10} at 1,663 and 1,651 cm^{-1} imply that the 30% loosely bound Q_B is reduced[13], whereas Q_A bands did not occur at all. In the amplitude spectrum of the 150-µs phase (**Fig. 5b**), Q_B bands of the hydrogen-bonded UQ_{10} disappeared (1,641 cm^{-1} (C=O), 1,615 cm^{-1} (C=C))[13,14] complementary to the Q_B^- band at 1,479 cm^{-1}, and smaller Q_A bands appeared (1,660, 1,628 and 1,601 cm^{-1})[11,12] complementary to the smaller Q_A^- bands at 1,466 and 1,447 cm^{-1}. In the amplitude spectrum of the 1.1-ms phase (**Fig. 5c**) Q_A carbonyl bands (1,660, 1,628 and 1,601 cm^{-1})[11,12] appeared due to Q_A^- oxidation. However, the carbonyl bands did not provide a fully complementary picture to the Q_A^- bands at 1,466 and 1,447 cm^{-1}, because only the band at 1,660 cm^{-1} increased, but not the bands at 1,628 and 1,601 cm^{-1}. The appearing Q_B carbonyl bands at 1,640 and 1,612 cm^{-1} did not decrease either at 1.1 ms compared to 150 µs as expected, even if the Q_B^- band at 1,479 cm^{-1} decreased. However, since in this spectral region the background absorption was very large, the intensities may vary due to phase errors and did not provide such a clear result as the more reliable marker bands of the C ··· O/C ··· C vibrations, which were not associated with such a high background absorption.

Carbonyl vibrations

In the 12-µs phase (**Fig. 5a**) two carbonyl bands appeared at 1,751 and 1,707 cm^{-1}. They represented protonation of an internal (1,751 cm^{-1}) and a water-exposed (1,707 cm^{-1}) carboxylic acid because both bands showed the typical frequency shift in D_2O (ref. 35). The assignment of the band at 1,707 cm^{-1} was not yet clear. In contrast, the band at 1,751 cm^{-1} was assigned below to Asp210 in the L subunit. The intensity of this band was further increased in the 150-µs phase (**Fig. 5b**), implying increasing extent of protonation. The positive band at 1,751 cm^{-1} in the 1.1-ms phase (**Fig. 5c**) indicated deprotonation. The band at 1,726 cm^{-1} in the 150-µs phase (**Fig. 5b**) indicated protonation of Glu212 in the L subunit[25,36]. In the 1.1-ms phase (**Fig. 5c**) the band at 1,724 cm^{-1} continued to increase, indicating that protonation of Glu212 in the L subunit continued in this phase.

The band at 1,736 cm^{-1} (**Fig. 5b,c**) was assigned to a free ester group of bacteriopheophytin (I)[37]. This band disappears because of the electrochromic shift of bacteriopheophytin caused by the reduction of Q_A[37]. Its reappearance, mainly in the 1.1-ms phase, is an additional marker for the reoxidation from Q_A^- to Q_A. This band was already observed in the 150-µs phase (**Fig. 5b**) as a result of partial reoxidation of Q_A^- but was three times larger in the 1.1-ms phase. This ratio was consistent with the amount of Q_A^- oxidation derived from the C ··· O/C ··· C vibrations of Q_A^-. This is an independent observation supporting late reoxidation of Q_A^- in the 1.1-ms phase.

Above 1,760 cm^{-1} a broad 'continuum' absorbance change appeared in the 1.1-ms phase (**Fig. 5c**). Such absorbance may indicate proton transfer via a chain of protonated internal water molecules in a Grotthuis-like mechanism as proposed for bacteriorhodopsin[38]. Proton transfer via water molecules within the extended water clusters has been discussed for the RC of *Rb. sphaeroides*[39].

Additional band assignments

The position of the bands at 1,113 and 1,093 cm^{-1} in the 12-µs phase (**Fig. 5a**) were consistent with vibration modes of a protonated and a

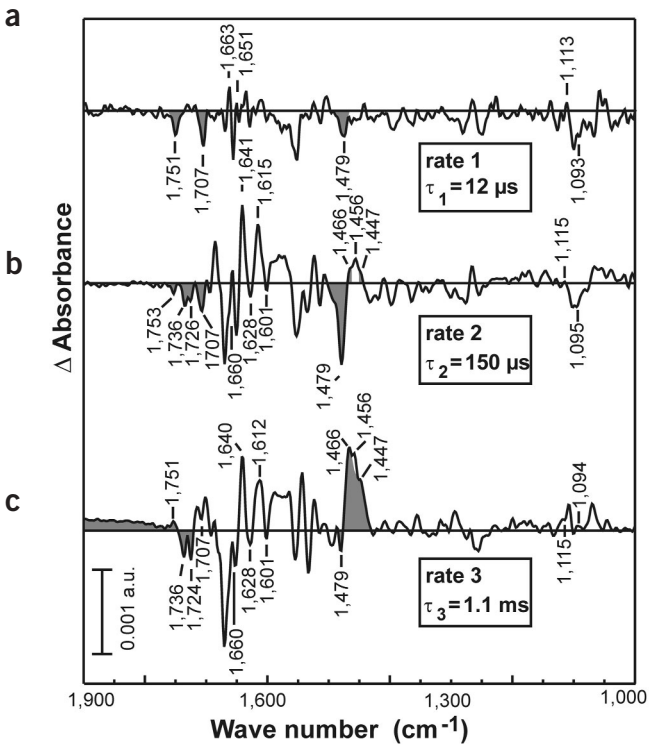

Figure 5 Amplitude spectra from 1,900 to 1,000 cm^{-1} for the three kinetic phases. (**a**) 12 µs. (**b**) 150 µs. (**c**) 1.1 ms.

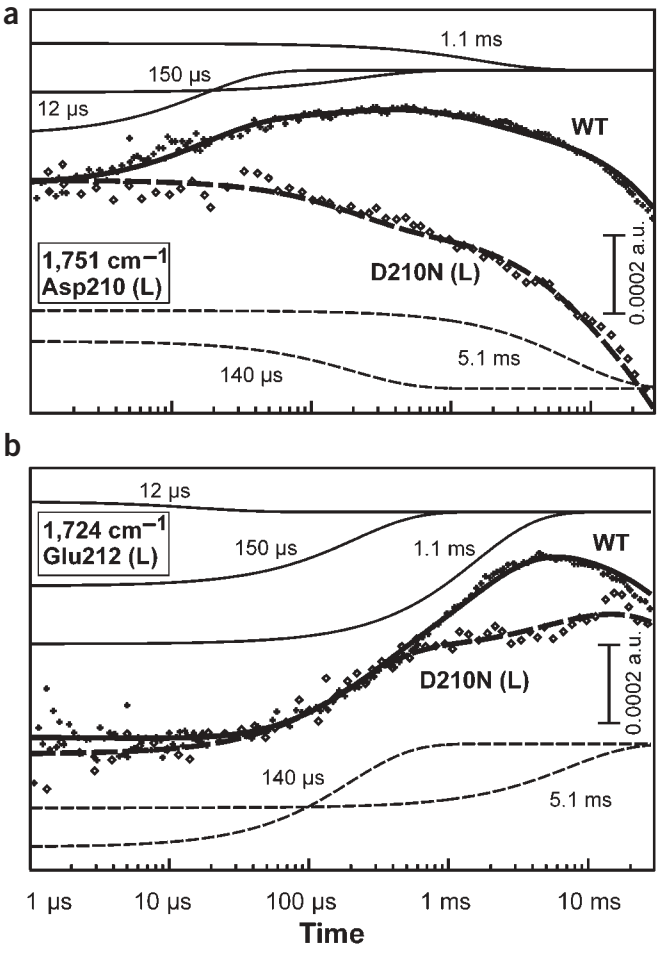

Figure 6 Comparison of wild-type and D210N (L) mutant kinetics in the $Q_A^-Q_B \rightarrow Q_AQ_B^-$ transition. (**a**) Absorbance changes at 1,751 cm^{-1} in wild type (crosses) and in the D210N (L) mutant RC (diamonds). In addition, the contributions of the single exponentials in wild type (solid line) and in D210N (L) (dashed line) are shown. The increase of the wild-type band for the 12 µs and 150 µs phases was no longer observed in D210N (L). (**b**) Absorbance changes at 1,724 cm^{-1} indicating protonation of Glu212 (L) are shown in wild-type (crosses) and in D210N (L) mutant RC (diamonds). In addition, the contributions of the single exponentials in wild type (solid line) and in D210N (L) (dashed line) are shown. Protonation of Glu212 (L) was still observed in the mutant, but the kinetics was changed.

neutral histidine, respectively[40,41]. The difference band 1,113 cm^{-1}/1,093 cm^{-1} indicates the disappearance of a neutral, π-protonated histidine and the appearance of a protonated histidinium cation, respectively. This histidine protonation might reflect the recently proposed proton uptake by His126 and His128 in the H subunit[42,43]. Unambiguous assignments for these bands would require experiments with additional histidine mutants; for now, we tentatively assign these bands to His126 and His128 in the H subunit. The protonation of a histidine continued in the 150-µs phase at 1,115 and 1,095 cm^{-1} (**Fig. 5b**). Although the band at 1,115 cm^{-1} was close to the noise level, it was reproduced in independent measurements. In the 1.1-ms phase (**Fig. 5c**) the band at 1,094 cm^{-1} appeared with positive sign, indicating deprotonation of the histidinium cation.

D210N mutant in the L subunit

Asp210 in the L subunit has been proposed to be involved into the proton uptake in the RC based on UV-VIS studies[44]. Therefore we investigated the $Q_A^-Q_B \rightarrow Q_AQ_B^-$ transition in the mutant D210N with step-scan FTIR spectroscopy. The reduction of Q_B prior to reoxidation of Q_A^- was more pronounced in the RC containing the D210N mutation in the L subunit. The majority of Q_B reduction observed at 1,479 cm^{-1} occurred with a time constant of 140 µs, whereas Q_A^- oxidation observed at 1,446 cm^{-1} mostly took place with a time constant of 5.1 ms (data not shown). The reoxidation of Q_A^- in the mutant was clearly slower than in wild type, and back reactions can be neglected. The charge recombination kinetics of D210N (at 57 ms and 1.7 s) are similar to those in wild type (data not shown). These results provide another piece of independent evidence for an intermediate between Q_A and Q_B.

Only the slowest phase was affected by a factor of ~5 in the mutant as compared with wild type, consistent with UV-VIS spectroscopic studies[44]. Very recently, Mezzetti *et al.*[45] have described the $Q_A^-Q_B \rightarrow Q_AQ_B^-$ transition in the D210N L subunit mutant using rapid-scan FTIR spectroscopy with 25-ms time resolution. With this slower time resolution, the $Q_A^-Q_B \rightarrow Q_AQ_B^-$ transition is not resolved and Q_B reduction at 140 µs prior to Q_A^- oxidation could not be observed.

Asp210 in the L subunit may be responsible for the band at 1,751 cm^{-1} (**Fig. 5**). If so, this band should be absent in the spectra for the RC containing the D210N L-subunit mutation. A comparison of the absorbance change at 1,751 cm^{-1} between the D120N L-subunit mutant and wild-type RC revealed that the increase of the carbonyl band at 12 µs and 150 µs observed in wild type was missing in the mutant (**Fig. 6a**); instead, the absorbance decreased at 140 µs and 5.1 ms. Therefore, the carbonyl band at 1,751 cm^{-1} in the $Q_A^-Q_B \rightarrow Q_AQ_B^-$ transition in the wild-type RC was assigned to the protonation of Asp210 in the L subunit. Nevertheless, we could not completely rule out that another nearby group, such as Asp17 in the M subunit, may be responsible for the protonation signal at 1,751 cm^{-1} and that mutation of Asp210 in the L subunit may induce a structural change that inhibits protonation of M subunit Asp17. Because mutation of Asp210 to asparagine does not induce a severe mutation, as the amplitude spectra show, we do not feel that such a possibility is likely. The carbonyl band of L-subunit Asp210 appeared only transiently and was therefore not resolved by static measurements[36,46].

The band at 1,724 cm^{-1} indicated protonation of Glu212 in the L subunit[25,36] (**Fig. 6b**). Notably, this residue became protonated mainly with the same time constant (1.1 ms) as Asp210 in the same subunit became deprotonated, suggesting that Asp210 transfers a proton to Glu212. In the L subunit D210N mutant, Glu212 still became protonated, but more rapidly than in wild type (with a time constant of 140 µs). It is possible that a different group might donate a proton in the mutant; for example, Asp17 (M) could substitute for Asp210 (L). Similar observations have been made in bacteriorhodopsin for Glu204 and Glu194 (ref. 38).

DISCUSSION

Three kinetic phases in $Q_A^-Q_B \rightarrow Q_AQ_B^-$ transition

The time-resolved step-scan FTIR measurements show that the $Q_A^-Q_B \rightarrow Q_AQ_B^-$ transition in RCs can be described by three apparent kinetic phases with time constants of 12 µs, 150 µs and 1.1 ms at 278 K. At room temperature the process is about three to four times faster than at 278 K. Thus, the 150-µs and 1.1-ms time constants agree with earlier UV-VIS and IR studies (~50 µs and ~200 µs at room temperature)[19,21,22,24,25,29]. The fastest phase at 12 µs has been observed by UV-VIS spectroscopy only in RCs reconstituted with menaquinone-10

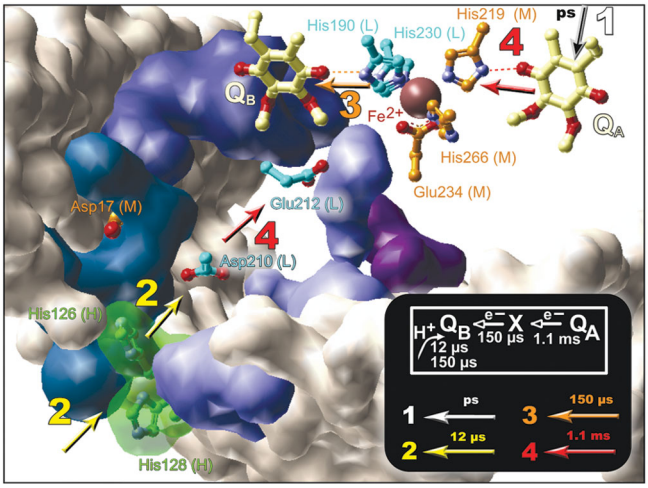

Figure 7 FTIR results in the context of the structural model (PDB entry 1AIG) [6]. Connolly description of the protein surface, gray; water-filled cavities inside the protein complex, blue. Generation of the $P^+Q_A^-$ charge-separated state within picoseconds (step 1) induces proton uptake by His126 and His128 in the H subunit at the entrance in the 12-µs phase (step 2); protonation of Asp210 in the L subunit within the proton-uptake pathway also occurs in this phase (step 2). Electrostatic changes in the environment of Q_B appear to induce the reduction of Q_B at the proximal position in the 150-µs phase (step 3). The electron is donated to Q_B by a not yet identified donor X. The His190 (L)-Fe^{2+}-His219 (M) moiety is optimally positioned for X. His219 (M) and His190 (L) are hydrogen bonded to Q_A and Q_B, respectively. Mutation of His219 (M) or exchange of the Fe^{2+} substantially alters the electron transfer from Q_A^- to Q_B (data not shown). The donor X^+ is reduced by Q_A^- in the 1.1-ms phase (step 4). Also in this phase, Asp210 (L) protonates Glu212 (L) (step 4). Glu212 (L) is the likely proton donor to Q_B after a second light-induced P oxidation.

at the Q_A site[21,22]. Thus, the present work is the first report on the fast rate of the $Q_A^-Q_B \rightarrow Q_AQ_B^-$ transition in RCs containing native quinones.

In contrast to previous interpretation[21,22], a noticeable electron transfer from Q_A^- to Q_B does not take place at 12 µs; the IR data show that after reduction of Q_A in the picosecond time range, proton uptake and protonation of aspartate or glutamate occur at 12 µs and 150 µs. In earlier investigations proton transfer has always been attributed to the slower time constants[19–22,24,25]. In addition, proton transfer has typically been assigned to transitions after Q_B has been reduced. Thus, the step-scan FTIR data show now that fast proton transfer in the microsecond time scale precedes Q_B reduction.

Our results are summarized in the context of the structural model (PDB entry 1AIG)[6] at the acceptor sites (**Fig. 7**). Proton uptake at the entrance of the proposed channel, probably by His126 and His128 in the H subunit, and by protonation of Asp210 in the L subunit inside the protein takes place mainly at 12 µs. These protonation changes seem to be induced by the reduction of Q_A. As proton uptake is also observed in RCs without Q_B occupancy[47], proton transfer seems to be independent of Q_B reduction. The protonation changes, especially the protonation of Asp210 in the L subunit, increase the positive-charge environment close to Q_B. The compensation of the positive charges seems to trigger the reduction of Q_B.

Q_B reduction prior to Q_A^- oxidation

UQ_{10} at Q_B is loosely bound to the RC as determined by binding affinity studies and observed in X-ray structural models in which Q_B was found at greatly varying positions[6,8–10]. Two Q_B binding sites have been identified in IR studies, one loosely bound with C=O vibrations at 1,663 and 1,651 cm^{-1} and the other hydrogen bonded with C=O vibrations at 1,641 cm^{-1} (ref. 13). X-ray studies have proposed a light-induced 5-Å movement of Q_B from a distal 'dark' to a proximal 'light' position relative to His190 in the L subunit, including a 180° propeller twist of the quinone ring[6]. It has been proposed that this movement represents a conformational gating for the $Q_A^-Q_B \rightarrow Q_AQ_B^-$ transition[6]. In the P209Y mutant in the L subunit, UQ_{10} only occupies the proximal 'light' position already in the dark-adapted state as shown by X-ray crystallography[10]. In this mutant, the 1- and 4-C=O vibrations of UQ_{10} at the Q_B binding site are observed only at 1,641 cm^{-1} (ref. 48). Therefore, the band at 1,641 cm^{-1} could be correlated with hydrogen-bonded UQ_{10} at the proximal 'light' position. This frequency is shifted as compared with unbound UQ_{10} as a result of hydrogen bonding of the 4-C=O group to His190 and of the 1-C=O group to Ser223 and Ile224, all three residues in the L subunit (**Fig. 7**). In the distal 'dark' position, Q_B is not hydrogen bonded and absorbs at 1,663 and 1,651 cm^{-1}, as in free UQ_{10}. If light induced a movement from the 'dark' to the 'light' position, it should be accompanied by frequency shift from 1,663 and 1,651 cm^{-1} to 1,641 cm^{-1} causing a difference band in the amplitude spectrum. Such a difference band does not appear; thus, a conformational movement from the distal 'dark' to the proximal 'light' position is excluded. In contrast, the reduction seems to be preceded by the fast proton uptake at 12 µs. Therefore, proton uptake—not the conformational gating of Q_B—seems to induce the Q_B reduction.

Our data indicate that a minor Q_B fraction is reduced at the distal position (1,663 and 1,651 cm^{-1}) at 12 µs, whereas the major Q_B fraction is reduced at the proximal position (1,641 cm^{-1}) at 150 µs.

Proton uptake by His126 and His128 in the H subunit and protonation of Asp210 in the L subunit proceed with a time constant of 150 µs. In the L subunit, Asp210 deprotonates and Glu212 protonates at 1.1 ms. Because these two residues are in close proximity, Glu212 is likely protonated by Asp210. This protonation seems to be a prerequisite for the reoxidation of Q_A^-. Proton transfer seems to take place mostly not through, but just between the large water-filled cavities (**Fig. 7**). In contrast, in bacteriorhodopsin proton transfer takes place through protonated water-filled cavities[49]. The water-filled cavities in RCs are about ten times larger than in bacteriorhodopsin (600 $Å^3$ versus 26 $Å^3$). These large units of less ordered water may be less suitable for proton transfer.

The intermediary electron donor X

On the basis of the data in this study, we propose that an additional electron donor X is necessary to reduce Q_B mainly at 150 µs. The oxidized form of the donor, X^+, will be reduced by Q_A^- with a time constant of 1.1 ms. The cofactor Fe^{2+}, coordinated by His190 in the L subunit and His219 in the M subunit, is located between Q_A and Q_B; this group of residues and cofactor is optimally positioned to function as X. Although the $Fe^{2+} \rightarrow Fe^{3+}$ transition has been excluded because Zn^{2+}-reconstituted reaction centers seem functional for electron transfer[18], preliminary FTIR experiments on Fe^{2+}-depleted RCs show dramatic changes in the $Q_A^-Q_B \rightarrow Q_AQ_B^-$ kinetics (data not shown). In addition, mutation of histidine ligated to Fe^{2+} disturbs the electron transfer kinetics (data not shown). These results suggest an important role for Fe^{2+} and its histidine ligands in the $Q_A^-Q_B \rightarrow Q_AQ_B^-$ transition.

The redox potential of Fe^{2+} in the structurally similar photosystem II is 400 mV (ref. 50), far above that expected in the RC (between –45 mV for Q_A and 20 mV for Q_B). Nevertheless, it is known that the redox potential can be varied in the required range by changing the

electron distribution of the ligands. Furthermore, the Fe^{2+} to Fe^{3+} change must only be transient, in the microsecond time range. A change of hydrogen bonds or of protonation could influence the redox potential of Fe^{2+}. In particular, His219 in the M subunit and His190 in the L subunit ligated to Fe^{2+} are hydrogen bonded to Q_A and Q_B, respectively. Actually, His219 in the M subunit is unusually strongly hydrogen bonded to the 4-C=O group of Q_A which is weakened in Q_A^- (ref. 11). Hydrogen bonding of 4-C=O of Q_B might be established after proton uptake, which could also modulate the redox potential of Fe^{2+}. Finally, another residue, Glu234 in the M subunit, which is ligated to Fe^{2+}, can also be protonated; its protonation state might also play a role in tuning the redox potential of the ferrous ion.

In principle, other functional groups such as a tyrosine or a tryptophan side chain could also function as X. However, no such residue is found at appropriate distances nor is redox potential of either group appropriate. Further experiments are necessary to establish whether Fe^{2+} has a structural role in stabilizing the Q_A and Q_B positions, or whether it is actively involved in electron transfer.

In summary, light-induced reduction of Q_A in the picosecond time range induces proton uptake at 12 µs. These protonation changes close to Q_B induce oxidation of X and reduction of Q_B at 150 µs. Q_B is reduced at its proximal light position and a propeller twist movement is not observed before reduction. The proton uptake rather than a conformational change seems to gate the $Q_A^-Q_B \rightarrow Q_AQ_B^-$ transition. Glu212 becomes protonated by Asp210 (both in the L subunit) and Q_A^- reduces X^+ at 1.1 ms.

The results show that time-resolved FTIR spectroscopy is able to resolve light-induced reactions in a 100-kDa protein at the atomic level over nine orders of magnitude, from 30 ns to 35 s.

METHODS

Sample preparation. Site-specific mutants were constructed as described[51] and modified[52]. RC protein was purified from *Rb. sphaeroides* R26 and from the mutant D210N (L), respectively, and reconstituted at the Q_B site by a 20-fold excess of UQ_{10} (ref. 53) to a final occupancy of at least 90% in wild type and ≥70% in D210N (L). Sample preparation for the IR measurements was carried out as described[11]. RCs (45 µl of 40 µM) dissolved in 10 mM Tris-HCl, 1 mM EDTA, 0.025% (w/v) LDAO, pH 8, were pipetted onto a CaF_2 window. After careful concentration under a gentle stream of nitrogen to a final volume of ~1 µl, the sample was sealed with another CaF_2 window and thermostabilized at 278 K in the FTIR apparatus.

FTIR measurements. The step-scan FTIR experiments were done in a vacuum FTIR spectrometer as described[28,29]. The spectra were recorded between 1,974 and 900 cm^{-1} with a spectral resolution of 7 cm^{-1}. We made a sample wheel that enabled the simultaneous measurement of eight IR samples. While the first sample relaxed back to the ground state, the sample wheel moved the next sample into the IR measuring beam. Thereby each sample relaxed for 40 s to ensure full recombination . The sample wheel can be thermostabilized between 268 K and 303 K. The reaction was started 0.8 s after the sample changer stopped by a Nd:YAG laser (532 nm, 7 ns, ~5 mJ). To improve the signal-to-noise ratio, 88–110 measurements of 8–10 different samples were averaged. Before and after each set of measurements rapid-scan FTIR measurements were taken[28,31] to check the sample activity and to collect data in the time range of ~10 ms to 35 s.

Global fit analysis. The data stored by two digital oscilloscopes providing ns and µs time resolution as well as the rapid-scan FTIR data were combined into one data set. This data set was kinetically analyzed using the global fit method[30]. In global fit analysis, absorbance changes (ΔA) are analyzed with sums of n exponentials with apparent rate constants k_i and amplitudes a_i (**Fig. 2**, ref. 30). As all absorbance changes between 1,900 and 1,000 cm^{-1} are analyzed simultaneously in this procedure, small absorbance changes with lower signal-to-noise ratios are guided by larger absorbance changes. This improves the quality of the fit procedure for smaller absorbance changes. A random distribution of the residuals around the baseline, a standard deviation close to 1 and a minor correlation of the time constants are criteria for an appropriate description.

ACKNOWLEDGMENTS

This work was financially supported by the Deutsche Forschungsgemeinschaft. We thank T.A. Egorova-Zachernyuk for providing RC sample material and D. Oesterhelt for providing the *Rb. sphaeroides* deletion strain *puf*ΔLMX21. We thank C. Fichtner for help in mutagenesis, C. Kandt for preparing Figures 1 and 7 and R. Goody for careful reading of the manuscript.

COMPETING INTERESTS STATEMENT

The authors declare that they have no competing financial interests.

Received 6 December 2002; accepted 11 June 2003
Published online 20 July 2003; doi:10.1038/nsb954

1. Okamura, M.Y., Paddock, M.L., Graige, M.S. & Feher, G. Proton and electron transfer in bacterial reaction centers. *Biochim. Biophys. Acta* **1458**, 148–163 (2000).
2. Gerwert, K. Molecular reaction mechanisms of proteins as monitored by time-resolved FTIR spectroscopy. *Curr. Opin. Struct. Biol.* **3**, 769–773 (1993).
3. Mäntele, W. Infrared and Fourier-transform infrared spectroscopy. In *Biophysical Techniques in Photosynthesis* (eds. Amesz, J. & Hoff, A.J.) 137–160 (Kluwer, Dordrecht, Netherlands, 1996).
4. Vogel, R. & Siebert, F. Vibrational spectroscopy as a tool for probing protein function. *Curr. Opin. Chem. Biol.* **4**, 518–523 (2000).
5. Barth, A. & Zscherp, C. What vibrations tell us about proteins. *Quart. Rev. Biophysics* **35**, 369–430 (2002).
6. Stowell, M.H.B. *et al.* Light-induced structural changes in photosynthetic reaction center: implications for mechanism of electron-proton transfer. *Science* **276**, 812–816 (1997).
7. Zouni, A. *et al.* Crystal structure of photosystem II from *Synechococcus elongatus* at 3.8 Å resolution. *Nature* **409**, 739–743 (1997).
8. Feher, G., Allen, J.P., Okamura, M.Y. & Rees, D.C. Structure and function of bacterial photosynthetic reaction centres. *Nature* **339**, 111–116 (1989).
9. Ermler, U., Fritzsch, G., Buchanan, S. & Michel, H. Structure of the photosynthetic reaction centre from *Rhodobacter sphaeroides* at 2.65 Å resolution: cofactors and protein-cofactor interactions. *Structure* **2**, 925–936 (1994).
10. Kuglstatter, A., Ermler, U., Michel, H., Baciou, L. & Fritzsch, G. X-ray structure analyses of photosynthetic reaction center variants from *Rhodobacter sphaeroides*: structural changes induced by point mutations at position L209 modulate electron and proton transfer. *Biochemistry* **40**, 4253–4260 (2001).
11. Brudler, R. *et al.* Asymmetric binding of the 1- and 4-C=O groups of Q_A in *Rhodobacter sphaeroides* R26 reaction centres monitored by Fourier transform infrared spectroscopy using site-specific isotopically labelled ubiquinone-10. *EMBO J.* **13**, 5523–5530 (1994).
12. Breton, J., Boullais, C., Burie, J.-R., Nabedryk, E. & Mioskowski, C. Binding sites of quinones in photosynthetic bacterial reaction centers investigated by light-induced FTIR difference spectroscopy: assignment of the interactions of each carbonyl of Q_A in *Rhodobacter sphaeroides* using site-specific ^{13}C-labeled ubiquinone. *Biochemistry* **33**, 14378–14386 (1994).
13. Brudler, R. *et al.* FTIR spectroscopy shows weak symmetric hydrogen bonding of the Q_B carbonyl groups in *Rhodobacter sphaeroides* R26 reaction centres. *FEBS Lett.* **370**, 88–92 (1995).
14. Breton, J., Boullais, C., Berger, G., Mioskowski, C. & Nabedryk, E. Binding sites of quinones in photosynthetic bacterial reaction centers investigated by light-induced FTIR difference spectroscopy: symmetry of the carbonyl interactions and close equivalence of the Q_B vibrations in *Rhodobacter sphaeroides* and *Rhodopseudomonas viridis* probed by isotope labeling. *Biochemistry* **34**, 11606–11616 (1995).
15. Holzapfel, W. *et al.* Initial electron-transfer in the reaction center from *Rhodobacter sphaeroides*. *Proc. Natl. Acad. Sci. USA* **87**, 5168–5172 (1990)
16. Gray, H.B. & Winkler, J.R. Electron transfer in proteins. *Ann. Rev. Biochem.* **65**, 537–561 (1995).
17. Moser, C.C., Page, C.C., Farid, R. & Dutton, P.L. Biological electron transfer. *J. Bioenerg. Biomembr.* **27**, 263–274 (1995).
18. Debus, R.J., Feher, G. & Okamura, M.Y. Iron-depleted reaction centers from *Rhodopseudomonas sphaeroides* R-26.1: characterization and reconstitution with Fe^{2+}, Mn^{2+}, Co^{2+}, Ni^{2+}, Cu^{2+}, and Zn^{2+}. *Biochemistry* **25**, 2276–2287 (1986).
19. Tiede, D., Vázquez, J., Córdova, J. & Marone, P.A. Time-resolved electrochromism associated with the formation of quinone anions in *Rhodobacter sphaeroides* R-26 reaction center. *Biochemistry* **35**, 10763–10775 (1996).
20. Graige, M.S., Feher, G. & Okamura, M.Y. Conformational gating of the electron transfer reaction $Q_A^-Q_B \rightarrow Q_AQ_B^-$ in bacterial reaction centers of *Rhodobacter sphaeroides* determined by a driving force assay. *Proc. Natl. Acad. Sci. USA* **95**, 11679–11684 (1998).
21. Li, J., Gilroy, D., Tiede, D. & Gunner, M.R. Kinetic phases in the electron transfer from $P^+Q_A^-Q_B$ to $P^+Q_AQ_B^-$ and the associated processes in *Rhodobacter sphaeroides* R-26 reaction centers. *Biochemistry* **37**, 2818–2829 (1998).
22. Li, J., Takahashi, E. & Gunner, M.R. $-\Delta G°_{AB}$ and pH dependence of the electron transfer from $P^+Q_A^-Q_B$ to $P^+Q_AQ_B^-$ in *Rhodobacter sphaeroides* reaction centers. *Biochemistry* **39**, 7445–7454 (2000).

23. Gerwert, K. Molecular reaction mechanisms of proteins monitored by time-resolved FTIR difference spectroscopy. In *Handbook of Vibrational Spectroscopy* (eds. Chalmers, J.M. & Griffiths, P.R.) (Wiley, Chichester, UK, 2001).
24. Hienerwadel, R. *et al.* Time-resolved infrared spectroscopy of electron transfer in bacterial photosynthetic reaction centers: dynamics of binding and interaction upon Q_A and Q_B reduction. *Biochemistry* **31**, 5799–5808 (1992).
25. Hienerwadel, R. *et al.* Protonation of Glu L212 following Q_B^- formation in the photosynthetic reaction center of *Rhodobacter sphaeroides*: evidence from time-resolved infrared spectroscopy. *Biochemistry* **34**, 2832–2843 (1995).
26. Uhmann, W., Becker, A., Taran, C. & Siebert, F. Time-resolved FT-IR absorption spectroscopy using a step-scan interferometer. *Appl. Spectrosc.* **45**, 390–397 (1991).
27. Burie, J.-R., Leibl, W., Nabedryk, E. & Breton, J. Step-scan FT-IR spectroscopy of electron transfer in the photosynthetic bacterial reaction center. *Appl. Spectrosc.* **47**, 1401–1404 (1993).
28. Rammelsberg, R., Hessling, B., Chorongiewski, H. & Gerwert, K. Molecular reaction mechanisms of proteins monitored by nanosecond step-scan FT-IR difference spectroscopy. *Appl. Spectrosc.* **51**, 558–562 (1997).
29. Brudler, R. & Gerwert, K. Step-scan FTIR spectroscopy of the Q_A–$Q_B \rightarrow Q_AQ_B$– transition in *Rb. sphaeroides* R26 reaction centres. *Photosynth. Res.* **55**, 261–266 (1998).
30. Hessling, B., Souvignier, G. & Gerwert, K. A model-independent approach to assigning bacteriorhodopsin's intramolecular reactions to photocycle intermediates. *Biophysical J.* **65**, 1929–1941 (1993).
31. Gerwert, K., Souvignier, G. & Hess, B. Simultaneous monitoring of light-induced changes in protein side-group protonation, chromophore isomerization, and backbone motion of bacteriorhodopsin by time-resolved Fourier-transform infrared spectroscopy. *Proc. Natl. Acad, Sci. USA* **87**, 9774–9778 (1990).
32. Brudler, R., Rammelsberg, R., Woo, T.T., Getzoff, E.D. & Gerwert, K. Structure of the I_1 early intermediate of photoactive yellow protein by FTIR spectroscopy. *Nat. Struct. Biol.* **8**, 265–270 (2001).
33. Nabedryk, E. *et al.* A protein conformational change associated with the photoreduction of the primary and secondary quinones in the bacterial reaction center. *FEBS Lett.* **266**, 59–62 (1990).
34. Kleinfeld, D., Okamura, M.Y. & Feher, G. Electron-transfer kinetics in photosynthetic reaction centers cooled to cryogenic temperatures in the charge-separated state: evidence for light-induced structural changes. *Biochemistry* **23**, 5780–5786 (1984).
35. Venyaminov, S.Yu. & Kalnin, N.N. Quantitative IR spectrophotometry of peptide compounds in water (H_2O) solutions. I. Spectral parameters of amino acid residue absorption bands. *Biopolymers* **30**, 1243–1257 (1990).
36. Nabedryk, E. *et al.* Fourier transform infrared difference spectroscopy of secondary quinone acceptor photoreduction in proton transfer mutants of *Rhodobacter sphaeroides*. *Biochemistry* **34**, 14722–14732 (1995).
37. Breton, J., Nabedryk, E., Allen, J.P. & Williams, J.A.C. Electrostatic influence of Q_A reduction on the IR vibrational mode of the 10a-ester C=O of H_A demonstrated by mutations at residues Glu L104 and Trp L100 in reaction centers from *Rhodobacter sphaeroides*. *Biochemistry* **36**, 4515–4525 (1997).
38. Rammelsberg, R., Huhn, G., Lübben, M. & Gerwert, K. Bacteriorhodopsin's intramolecular proton-release pathway consists of a hydrogen-bonded network. *Biochemistry* **37**, 5001–5009 (1998).
39. Lancaster, C.R.D. & Michel, H. The coupling of light-induced electron transfer and proton uptake as derived from crystal structures of reaction centres from *Rhodopseudomonas viridis* modified at the binding site of the secondary quinone, Q_B. *Structure* **5**, 1339–1359 (1997).
40. Noguchi, T., Inoue, Y. & Tang, X.-S. Structure of a histidine ligand in the photosynthetic oxygen-evolving complex as studied by light-induced Fourier transform infrared difference spectroscopy. *Biochemistry* **38**, 10187–10195 (1999).
41. Hasegawa, K., Ono, T. & Noguchi, T. Vibrational spectra and *ab initio* DFT calculations of 4-methylimidazole and its different protonation forms: infrared and raman markers of the protonation state of a histidine side chain. *J. Phys. Chem. B.* **104**, 4253–4265 (2000).
42. Axelrod, H.L., Abresch, E.C., Paddock, M.L., Okamura, M.Y. & Feher, G. Determination of the binding sites of the proton transfer inhibitors Cd^{2+} and Zn^{2+} in bacterial reaction centers. *Proc. Natl. Acad, Sci. USA* **97**, 1542–1547 (2000).
43. Ädelroth, P. *et al.* Identification of the proton pathway in bacterial reaction centers: decrease of proton transfer rate by mutation of surface histidines at H126 and H128 and chemical rescue by imidazole identifies the initial proton donors. *Biochemistry* **40**, 14538–14546 (2001).
44. Paddock, M.L. *et al.* Identification of the proton pathway in bacterial reaction centers: cooperation between Asp-M17 and Asp-L210 facilitates proton transfer to the secondary quinone (Q_B). *Biochemistry* **40**, 6893–6902 (2001).
45. Mezzetti, A. *et al.* Rapid-scan Fourier transform infrared spectroscopy shows coupling of Glu-L212 protonation and electron transfer to Q_B in *Rhodobacter sphaeroides* reaction centers. *Biochim. Biophys. Acta* **1553**, 320–330 (2002).
46. Nabedryk, E., Breton, J., Okamura, M.Y. & Paddock, M.L. Simultaneous replacement of Asp-L210 and Asp-M17 with Asn increases proton uptake by Glu-L212 upon first electron transfer to Q_B in reaction centers from *Rhodobacter sphaeroides*. *Biochemistry* **40**, 13826–13832 (2001).
47. Maróti, P. & Wraight, C.A. Flash-induced H^+ binding by bacterial photosynthetic reaction centers: comparison of spectrophotometric and conductimetric methods. *Biochim. Biophys. Acta* **934**, 314–328 (1988).
48. Breton, J. *et al.* Vibrational spectroscopy favors a unique Q_B binding site at the proximal position in wild-type reaction centers and in the Pro-L209 → Tyr mutant from *Rhodobacter sphaeroides*. *Biochemistry* **41**, 12921–12927 (2002).
49. Spassov, V.Z., Luecke, H., Bashford, D. & Gerwert, K. pKa calculations suggest storage of an excess proton in a hydrogen-bonded water network in bacteriorhodopsin. *J. Mol. Biol.* **312**, 203–219 (2001).
50. Nugent, J.H.A. Oxygenic photosynthesis—electron transfer in photosystem I and photosystem II. *Eur. J. Biochem.* **237**, 519–531 (1996).
51. Farchaus, J.W. & Oesterhelt, D. A *Rhodobacter sphaeroides* puf L, M and X deletion mutant and its complementation in trans with a 5.3 kb puf operon shuttle fragment. *EMBO J.* **8**, 47–54 (1989).
52. Remy, A. Der $Q_A^-Q_B \rightarrow Q_AQ_B^-$-Übergang im bakteriellen photosynthetischen Reaktionszentrum von *Rhodobacter sphaeroides*. Thesis, Ruhr-University Bochum, Bochum, Germany (2002).
53. Okamura, M.Y., Isaacson, R.A. & Feher, G. Primary acceptor in bacterial photosynthesis: obligatory role of ubiquinone in photoactive reaction centers of *Rhodopseudomonas spheroides*. *Proc. Nat. Acad. Sci. USA* **72**, 3491–3495 (1975).